ELECTRONIC SUPPORTING INFORMATION

Impact of intracellular metallothionein on metal biouptake and partitioning dynamics at bacterial interfaces

Romain M. Présent,[1,2] Elise Rotureau,[*,1,2] Patrick Billard,[1,2] Christophe Pagnout,[3,4] Bénédicte Sohm,[3,4] Justine Flayac,[3,4] Renaud Gley,[1,2] José P. Pinheiro,[1,2] and Jérôme F. L. Duval[*,1,2]

[1] CNRS, LIEC (Laboratoire Interdisciplinaire des Environnements Continentaux), UMR7360, Vandoeuvre-lès-Nancy F-54501, France.

[2] Université de Lorraine, LIEC, UMR7360, Vandoeuvre-lès-Nancy F-54501, France.

[3] CNRS, LIEC (Laboratoire Interdisciplinaire des Environnements Continentaux), UMR7360, Campus Bridoux, Metz F-57070, France.

[4] Université de Lorraine, LIEC, UMR7360, Campus Bridoux, Metz F-57070, France.

Outline of the ESI content:

Section A: Determination of cell volume fraction φ. A1. Bacteria imaging using Atomic Force Microscopy (AFM). A2. Evaluation of the relationship between OD_{600} and cell concentration.
Section B: Electrokinetic measurements.
Section C: Electroanalytical measurements. C1. Preparation of the thin mercury film electrode (TMFE). C2. AGNES and SCP measurement principles. C3. Experimental protocol for electrochemical measurements.
Section D: Addressing metal biosurface sorption as a function of cell volume fraction φ. D1. Quantification of adsorbed cadmium amount at the biosurface using Ligand Exchange Technique. D2. Metal adsorption measurements *versus* φ and conclusions.
Section E: Details on purification of MBP-MT.
Section F: Determination of Cd(II)-MTc complex stability constant from electrochemical measurements.

Section G: Construction of a master curve from Cd(II) depletion kinetic data collected for JW3434 cells (Figure 1A).

5 Figures (Figures S1-S5). References applying to this document are mentioned at the end of the document.

Section A: Determination of cell volume fraction φ.

Cell volume fraction φ was evaluated from bacterial size as determined from atomic force microscopy (AFM) imaging of cells (§A1) and from the relationship, derived from cytometry measurements, that exists between OD_{600} and cells concentration in solution (§A2).

A1. Bacteria imaging using Atomic Force Microscopy (AFM).

The bacterial strains JW3434 and JW3434-MTc were first imaged in HMM liquid media using AFM in peak force tapping mode. For that purpose, glass slides were first coated using 0.1% polyethylenimine (PEI) and then rinsed with ultrapure water. A drop solution containing bacterial cells was deposited onto the PEI-coated glass slides, allowed to rest for 30 minutes and subsequently rinsed with weakly complexing HMM medium. Bacterial cells were then imaged at room temperature with a Dimension FastScan AFM (Bruker AXS, Palaiseau, France) at a frequency of 2 kHz and a scan rate of 1 Hz, using silicon nitride AFM tips with nominal spring constant of 0.24 N/m (SNL, Brucker, Palaiseau). Cross section measurements performed on about 10 cells for JW3434 and 40 cells for JW3434-MTc revealed that *E. coli* strains are rod-shaped cells with lengths and diameters of *ca.* 2.5 µm and 0.7 µm for JW3434 and 3.1 µm and 0.82 µm for JW3434-MTc, respectively. An illustrative example is provided in **Figure S1**. For the sake of simplicity, bacteria were assimilated to spheres with an equivalent radius found to be *ca.* 670 nm and 795 nm for JW3434 and JW3434-MTc, respectively.

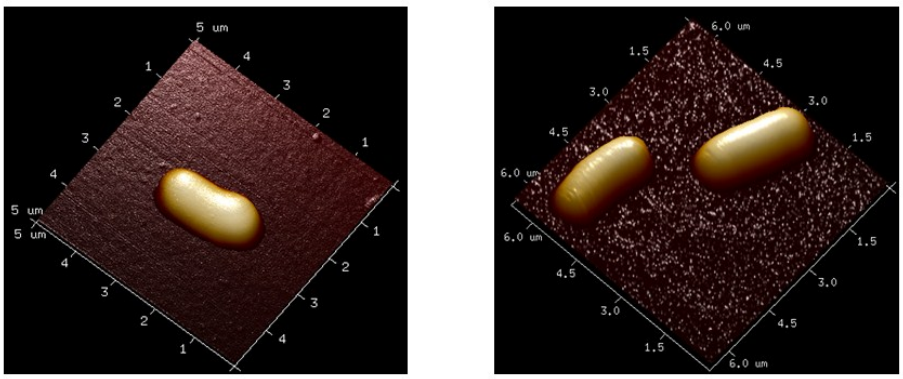

Figure S1. AFM images of JW3434 (left) and JW3434-MTc (right) obtained in HMM medium.

A2. Evaluation of the relationship between OD_{600} and cell concentration.

The equivalency between a measured optical density OD_{600} of unity and the number of bacterial cells per unit volume was determined from cell counting by flow cytometry (C6 Accuri, BD Biosciences). Results demonstrate that an optical density OD_{600} of 1 corresponds to 8×10^8 cells/ml for both JW3434 and JW3434-MTc strains. A series of cell suspensions diluted from a fresh cell culture was then prepared in weakly metal complexing HMM medium and the corresponding absorbance was measured for each cell suspension at 600 nm (OD_{600}). A linear relationship between OD_{600} and cell concentrations was obtained for OD_{600} values lower than unity. For larger density values, the corresponding cell volume concentration was estimated from the cubic spline interpolation of OD_{600} measured at larger cell concentrations. The volume fraction φ involved in the theory outlined in §2 of the main text was then simply evaluated from cell density c_p (m^{-3}) on the basis of the relationship $\varphi = V_p \times c_p$ where V_p stands for the volume of an individual bacterium assimilated to a sphere with equivalent radius obtained from AFM imaging.

Section B: Electrokinetic measurements.

Fresh cell suspensions were centrifuged at 3000 rpm, bacterial cells were then washed with HMM medium and subsequently dispersed at a volume fraction of *ca.* 4×10^{-3} % in $NaNO_3$ electrolyte solutions of concentration 1 mM to 200 mM. **Figure S2** displays the measured electrophoretic mobility μ of JW3434 (●) and JW3434-MTc (●) cells at pH 6.8 over the above range of salinity conditions (measurements details as in [1]). In qualitative agreement with predictions from soft surface electrokinetic theory[2] cell electrophoretic mobility decreases in magnitude with increasing electrolyte concentration as a result of cell surface charge screening by ions from solution. For electrolyte concentration above *ca.* 100 mM, μ reaches a non-zero plateau value that reflects (i) the hydrodynamic softness (*i.e.* ion and water-permeabilities) of the cell membrane, and (ii) a complete screening of cell surface electrostatics.[2–4] **Figure S2** further highlights that JW3434 and JW3434-MTc strains exhibit similar electrokinetic features. The conductivity of the HMM medium under the conditions adopted for metal depletion kinetic measurements is 10 mS cm^{-1}, which corresponds to an equivalent concentration of $NaNO_3$ salt of about 110 mM. **Figure S2** indicates that for such solution salinity level, cell electrostatics is fully screened, which justifies our setting $\beta_a = 1$ in the main text where β_a is the factor for Boltzmann accumulation of metal ions at the cell membrane surface (see §2 in the main text). In addition, AFM imaging did not reveal any protruding soft peripheral surface structures for the cells of interest in this work, which further validates the equality $\bar{f}_{el} = 1$ adopted for the modeling of the data displayed in **Figure 1** of the main text.

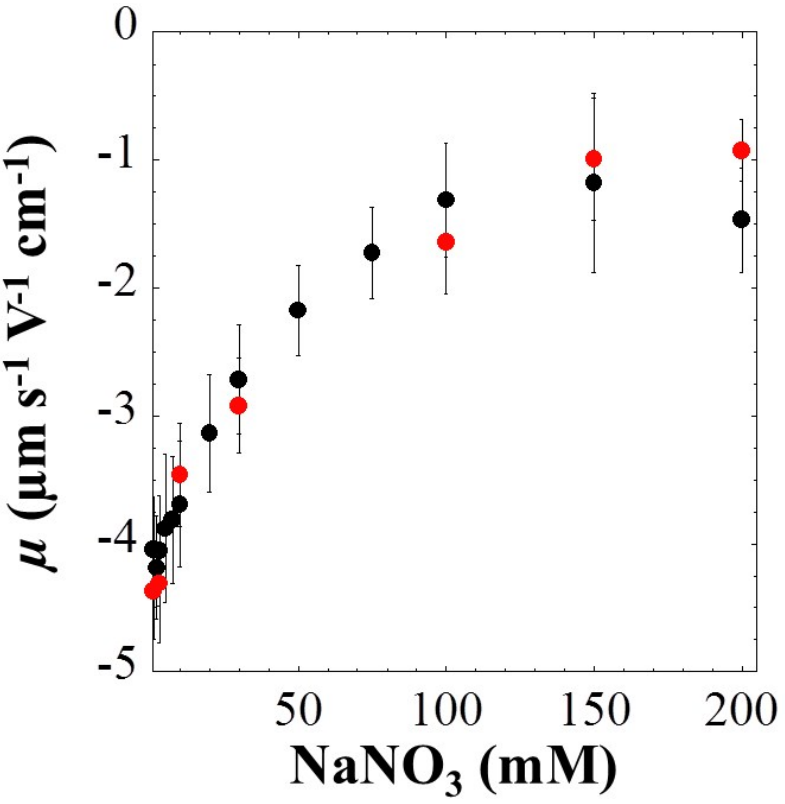

Figure S2. Dependence of the electrophoretic mobility μ on $NaNO_3$ electrolyte concentration for JW3434 (●) and JW3434-MTc cells (●). Metal depletion kinetic experiments (**Figure 1** in the main text) were performed in HMM medium that corresponds to a 110 mM equivalent concentration of $NaNO_3$.

Section C: Electroanalytical measurements.

C1. Preparation of the thin mercury film electrode (TMFE).

The preparation of the TMFE starts with polishing and electrochemical pretreatments as detailed elsewhere.[5] Then, a thin mercury film was plated *ex situ* on the glassy carbon (GC) electrode *via* electrodeposition at -1.3 V (with respect to Ag/AgCl), at 1000 rpm for 240 s in a 0.48 mM mercury (II) nitrate solution under acidic conditions (0.75 mM HNO_3, pH 1.9). Once the experiments completed, the TMFE was cleaned using successive mercury reoxidations in 80 mM ammonium thiocyanate solution buffered with ammonium acetate (pH = 3.4).

C2. AGNES and SCP measurement principles.

Absence of gradients and Nernstian equilibrium stripping (AGNES) measurements allows the measurement of concentration of free metal ions in a given solution. The reader is referred to the paper by Domingos *et al.*[6] for extensive details. Briefly, AGNES technique consists of two steps, a metal deposition and a metal reoxidation step. The deposition step is performed according to two stages: (i) a potential $E_{1,a}$ (-0.75 V *vs.* Ag/AgCl) corresponding to conditions where metal deposition process is diffusion-limited, is applied for a time $t_{1,a}$ (40 s) while stirring at a rotation speed of 1000 rpm, and (ii) a potential $E_{1,b}$ (-0.655 V *vs.* Ag/AgCl) is then applied for a delay $t_{1,b}$ set equal to $3t_{1,a}$ (120 s, with stirring) in order to reach the specific situation where absence of metal concentration gradient between the solution in the vicinity of the electrode and inside the mercury film is obtained. Then, a constant oxidizing current I_s (3 µA) is applied until the potential reaches a value well beyond the reoxidation transition plateau (-0.4 V *vs.* Ag/AgCl for Cd(II)). The signal representing the time required for reoxidation is measured and leads to the determination of the amount of metal deposited in the first step of the procedure, and this deposited metal amount is then proportional to the searched free metal concentration in bulk solution.[7]

The determination of the total amount of metal species in solution is performed using stripping chronopotentiometry (SCP), also a two-step electrochemical technique. A first step consists in the deposition of metal in the TMFE *via* application of a single potential E_1 (-0.75 V *vs.* Ag/AgCl) for a time delay t_d of 45 s. Then, a constant oxidizing current I_s (3µA) is applied until the potential reaches a value well beyond the reoxidation transition plateau (0.4 V *vs.* Ag/AgCl) for Cd). Similarly to AGNES, analytical signal representing the time required for metal reoxidation is measured and leads to the evaluation of the concentration of free and labile metal concentrations in solution. 'Labile' refers here to all metal complex species (*i.e.* formed between metals and ligands -if present- in solution) that may contribute to the SCP signal due to their fast association/dissociation as compared to the timescale of the experiment

(identified here with the timescale required to establish a steady-state diffusion layer in the vicinity of the metal-consuming electrode[8]). It can be legitimately assumed that the fraction of metal ions adsorbed at the bacterial cell walls does not contribute to the measured electrochemical signal due to the very slow diffusion of the bacteria from solution to the electrode (*i.e.* the 'metal-cell complexes' can be viewed as inert within the timescale of the experiments).

C3. Experimental protocol for electrochemical measurements.

A disposable polystyrene cell was placed in a double-walled container thermostated by a refrigerating-heating water circulator to regulate temperature at 35°C with an accuracy of ± 0.1°C during electrochemical measurements. Batch solution of poor metal-complexing medium (HMM) was prepared at pH 4, which ensured that all metal is in free form. Prior to measurements in the presence of bacterial cells, electrochemical calibration with 5×10^{-7} M, 10^{-6} M or 2×10^{-6} M metal concentration solution (ultra-pure certified $Cd(NO_3)_2$, Fluka) was systematically performed. 10 mins prior to the start of SCP or AGNES measurements, nitrogen bubbling was used to remove oxygen from solution. After completion of the calibration, pH was fixed to 6.8 upon addition of 1 M NaOH. Under such conditions, 85% of the total cadmium content is present in free form, a conclusion obtained from V-Minteq thermodynamic metal speciation evaluation.[9] The remaining 15% is mainly engaged in complexes formed with nitrate and chloride anions. In line with the results described elsewhere,[9] free Cd(II) metal ions are considered as the only bioactive species. Then, two electroanalytical methods were employed to follow the decrease over time of the metal ions concentration in the bulk solution as a result of metal biouptake and metal adsorption at the cells surface: Stripping Chronopotentiometry (SCP, see §C2) and Absence of Gradient and Nernstian Stripping (AGNES, §C2). The former allows the measurement of the free and labile metal complexes while the latter enables the detection of the only free metal ions fraction.

Analysis of the results obtained from these two techniques thus makes it possible to identify changes in metal speciation over time. Under the conditions adopted in this study, AGNES and SCP results were similar within analytical uncertainties, thus evidencing the absence of significant changes in metal speciation in the course of biouptake experiments. This therefore excludes the possible excretion of metal complexing ligands by the bacteria. In view of these elements, only SCP results are reported in this work.

Section D: Addressing metal biosurface sorption as a function of cell volume fraction φ.

D1. Quantification of adsorbed cadmium amount at the biosurface using Ligand Exchange Technique.

A set of 40 ml HMM batch solutions containing 1.91×10^{-6} M Cd(II) were prepared as detailed in the main text and bacterial cells were then added into each solution. After 2, 10, 30, 60 and 180 min cell contact with the metal-containing solution, half of the samples were 0.2 µm filtered in order to remove bacterial cells. For the other half, 2 ml of 0.01 M ethylenediaminetetraacetic acid (EDTA) solution was added and vortexed for 1 min. After a delay of 10 min, solutions were then filtered and acidified. The Cd(II) content in all solution samples was subsequently determined by atomic absorption flame spectroscopy (Varian 220FS). Analysis of the first series of solutions provided the bulk concentration of Cd(II) and analysis of the second series allowed evaluation of the sum of the concentration of metals adsorbed at the cell surface plus that of metals in bulk solution, recalling here that EDTA is a suitable competing ligand for the determination of the adsorbed metal amount at biosurfaces.[10]

D2. Metal adsorption measurements *versus* φ and conclusions.

As extensively detailed in the main text (see **Figure 2** therein), the metal amount adsorbed at the total biosurface developed in cells suspension remains constant with time. This conclusion is derived from AAS measurements (see §D1) performed on a sample with given cell volume fraction φ, and it is in line with the results independently obtained from electrochemical measurements (**Figure 2**). To further support this conclusion over the whole range of φ conditions tested in **Figure 1**, we report in **Figure S3** the bulk metal concentration drop $c_{\mathrm{M}}^{*}(0)-c_{\mathrm{M}}^{*}(0^{+})$ as detected by electrochemistry immediately after addition of cells in the metal-containing HMM medium. In case of a constant adsorbed amount of metal ions per unit cell surface area with time, it is straightforward to verify that $c_{\mathrm{M}}^{*}(0)-c_{\mathrm{M}}^{*}(0^{+})$ must satisfy the relationship $c_{\mathrm{M}}^{*}(0)-c_{\mathrm{M}}^{*}(0^{+})=3\Gamma\varphi/a$ where Γ is the surface concentration of adsorbed metals per unit cell surface area. The linear dependence of $c_{\mathrm{M}}^{*}(0)-c_{\mathrm{M}}^{*}(0^{+})$ on φ is well confirmed by **Figure S3** for both strains and slope analysis provides $\Gamma = 1.8 \times 10^{-7}$ mol m^{-2} and $\Gamma = 7.5 \times 10^{-8}$ mol m^{-2} for JW3434 and JW3434-MTc cells, respectively.

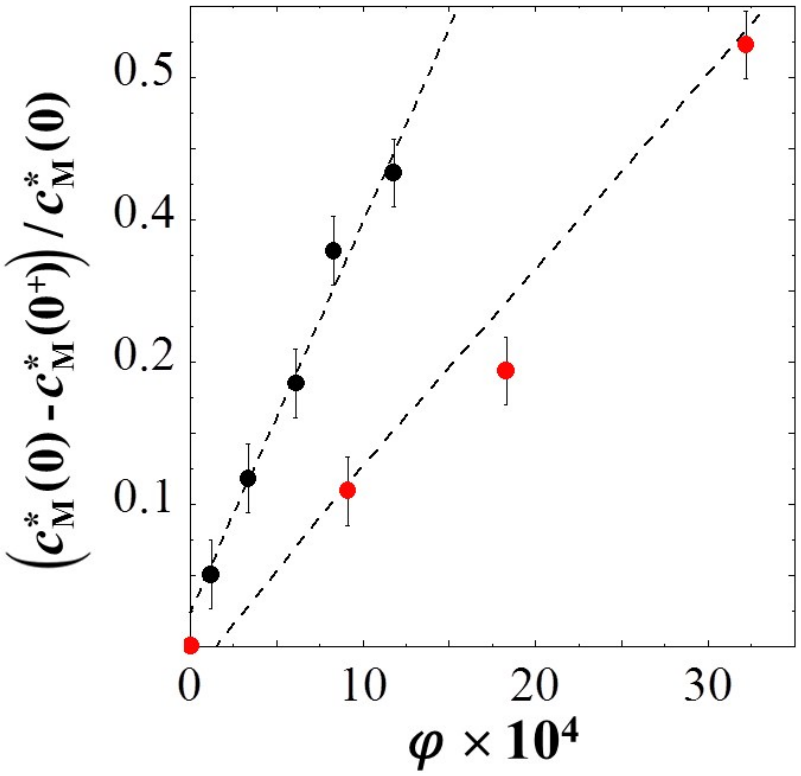

196

197 **Figure S3.** Dependence of $\left(c_M^*(0) - c_M^*(0^+)\right) / c_M^*(0)$ on cell volume fraction φ where $c_{M,total}^*$ is the
198 total metal concentration in solution for JW3434 (●) and for JW3434-MTc (●). Data were derived
199 from SCP electrochemical measurements (see text for details).

200

201 ## Section E: Details on purification of MBP-MT.

202 JW3434-MTc cells were grown overnight at 37°C to 4 × 10^8 cells/ml (OD_{600} ≃ 0.5) in 200
203 ml rich broth (10% tryptone (w/v), 5% yeast extract (w/v), 2% glucose (w/v)) in the presence
204 of ampicillin at 100 µg/ml concentration. Then, cells were incubated at 37°C for 2 hours with
205 the addition of IPTG at a final concentration of 0.3 mM (in order to optimize the production
206 of MBP-MT). For the sake of completeness, growth cultures of JW3434-MTc without IPTG
207 and of JW3434 with IPTG were processed to confirm the absence of induction of intracellular
208 MTc under such conditions. Cells were harvested by centrifugation at 4000 g for 20 mins,
209 resuspended in 5 ml of Column Buffer (20 mM Tris, pH 7.4, 200 mM NaCl) and frozen at -
210 20°C overnight. Then, cells were thawed in cold water and lysed by French press (1 KBar).

Extracts obtained were centrifuged at 20000 × g for 30 mins at 4°C and supernatants were collected. Total protein concentrations were determined following the Bradford method.[11] MBP-MT was purified by affinity-chromatography on an amylose column following instructions by the manufacturer (New England Biolabs) without EDTA in Column Buffer. Then, ten fractions of 0.6 ml were collected at a satisfactory purity as controlled by SDS-PAGE. MBP-MT suspension was then dialyzed in Tris buffer (50 mM Tris, pH 7.4) with 10 kD tubing (SpectrumLabs) and concentrated using 3 kD Amicon Centrifugal Filter Unit (Millipore) at 4000 g for 10 mins. Finally, MBP-MT suspension was stored at -20°C at a minimum concentration of 1 mg/ml in 30% glycerol. The purification yield was 12.75 mg of MBP-MT per liter of culture, thus leading an intracellular weight of MBP-MT (50 kDa) equal to 1.12×10^{-14}g/cell. As thiol groups are mainly involved in metal sequestration processes, intracellular cysteine number brought by the MBP-MT complex was determined from analysis of the nucleotide sequence. As a result, we found that 20 thiol groups are supported by a single MBP-MT. Accordingly, making use of the molecular weight and mass concentration of MBP-MT per cell as indicated above, the intracellular thiol concentration stemming from intracellular MBP-MT is estimated at 2.1 mM.

Section F: Determination of nanoparticulate Cd(II)-MTc complex stability constant from electrochemical measurements.

From the theoretical analysis of bulk metal depletion kinetic data (**Figure 1B** in the main text), we derived the magnitude of the stability constant $\overline{K}^*$ for nanoparticulate Cd(II)-MTc complexes (**Table 1** in the main text**)**. Cd(II) in the intracellular cell medium bind preferably to sulfide and thiol groups due to their high affinity to such ligands. Accordingly, the effective complexation constant $\overline{K}^*$ should reflect the complexation of intracellular Cd with the total amount of thiol groups supported by the proteins present in the intracellular volume. In the

literature, the total thiol content in a *Escherichia coli* strain similar to that used in this work but lacking intracellular MTc was quantified and estimated to be 9-10 mM.[12] Consequently, for the JW3434-MTc strain of interest here the total intracellular concentration of thiol groups stemming from MBP-MT and from other cytosolic proteins is ca. 12 mM. To confirm $\bar{K}^*$ value as derived from the quantitative interpretation of Cd(II) depletion kinetic features (**Figure 1B**), we attempted an independent evaluation of $\bar{K}^*$ from electrochemical measurements performed in a reconstructed intracellular cytosol-like medium upon successive additions of metal ions. For the sake of realism and to best mimic the conditions prevailing in a living bacterium, the cytosol-like medium consisted of the total amount of MBP-MT and of the other pool of proteins mixed at a representative concentrations ratio applying in real cytosolic medium (pH = 7.0). It is here recalled that intracellular concentration of MBP-MT was determined in Section E and that the concentration of the other intracellular proteins can be derived in a first approximation from the intracellular concentration of thiol groups as reported elsewhere.[12] The intracellular concentrations of metal ions relevant over the range of cell volume fractions tested in **Figure 1B** directly follows from theory and more specifically from the corresponding values of $\phi_u^T = \phi_u^c + \phi_u^M$ (with ϕ_u^c and ϕ_u^M defined in §2 of the main text) theoretically evaluated under equilibrium conditions reached at $t \to \infty$. In details, for a given ϕ_u^T (expressed in mol m^{-2}) the corresponding intracellular concentration of metal ions in mol m^{-3} is simply defined by $\phi_u^T S_a / V_p$ with S_a and V_p the surface and volume of an individual bacterium, respectively. However, due to the so-obtained high concentrations of Cd(II) and proteinaceous components in the reconstructed cytosolic medium (which made the electrochemical measurements difficult to perform), we had to reduce by a factor 100 the above concentrations upon keeping the concentration ratios between the various components to magnitudes in line with those applying in true intracellular medium. In details, the purified MTc and the total extracted cytosolic proteins concentrations in the cytosol-like medium were

adjusted so that the ratio between concentration of thiol groups from MTc and that prevailing in the cytosolic compartment is 0.2 (*i.e.* 2 mM/10 mM where 2mM and 10 mM values were derived above). Accordingly, adopted concentrations of MTc and of total extracted cytosolic proteins in the reconstructed medium used for electroanalytical measurements are 0.05 g/L and 0.47 g/L, respectively. Although a precise value of the total ionic strength in intracellular bacterial medium is difficult to evaluate due to its inherent composition complexity, Lodish et al[13] listed the intracellular concentrations of major ions in *Escherichia coli* from which we estimated an intracellular total ionic strength of 150 mM (computed with use of Vminteq speciation code). Therefore, complexation experiments of Cd(II) by purified MBP-MT and other cytosolic proteins were performed in a 150 mM $NaNO_3$ electrolyte solution at 35°C. Measurements in such physico-chemical medium conditions were performed following the procedure detailed in Section C. The results are reported in **Figure S4** below and they reveal that the obtained magnitude of $\bar{K}^*$ is in remarkable agreement with that derived from the refined analysis of kinetics of Cd(II) bulk depletion solution (**Figure 1B**, **Table 1**) in suspensions of JW3434-MTc. AGNES measurements (**Figure S4**) show a *ca.* 2-fold increase of $\bar{K}^*$ at low metal to ligand ratios $(\phi_u^T S_a / V_p) / \rho_S^{V_i}$ (or equivalently high φ) as compared to $\bar{K}^*$ values derived at high ratio $(\phi_u^T S_a / V_p) / \rho_S^{V_i}$ (or equivalently low φ). It is stressed that the analysis of the bulk metal depletion data (**Figure 1B)** at high φ where $c_M^*(t \to \infty) \to 0$ provides only lowest estimates of $\bar{K}^*$ as these data fall within the regime $\bar{K}^* >> 1$ for which complete depletion of M from solution is achieved.[14] Additional complexation measurements performed in the presence and absence of proteins other than MTc reveal that metal binding by MTc dominates in intracellular cell medium.

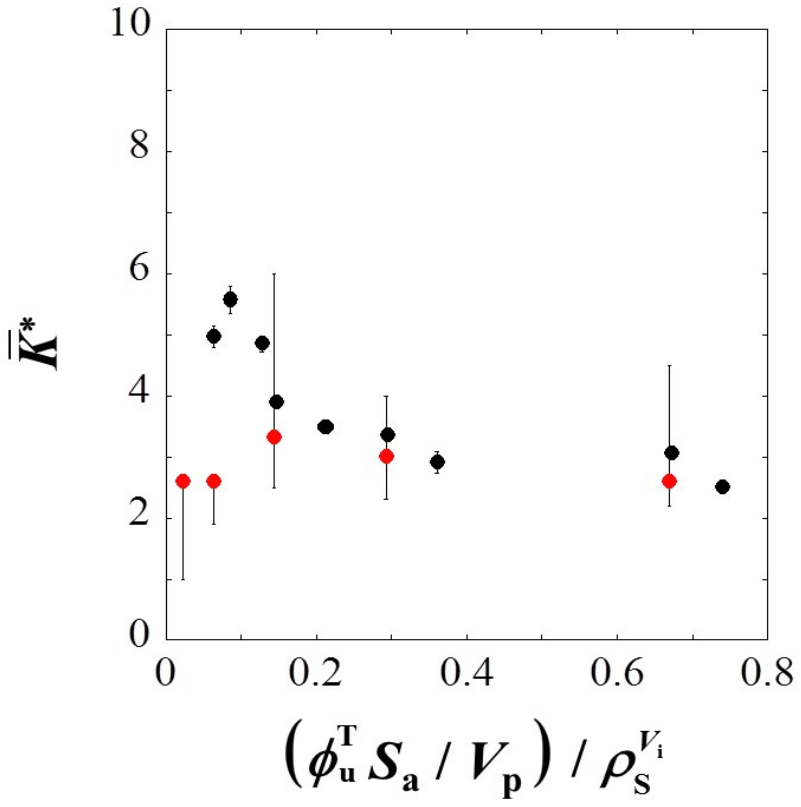

283

284 **Figure S4.** $\bar{K}^*$ values obtained from the analysis of bulk metal depletion kinetics (●) and from
285 AGNES measurements in a reconstructed cytosolic medium (●), where bulk Cd(II) concentration is
286 fixed to the value $\phi_u^T S_a / V_p$ reached at equilibrium ($t \to \infty$) under the cell volume fraction conditions
287 specified in **Figure 1B**. Values of $(\phi_u^T S_a / V_p) / \rho_S^{V_i}$ for $\varphi = 2.03\times10^{-4}$, 4.23×10^{-4}, 9.13×10^{-4} and 1.83×10^{-3}
288 are 0.67, 0.30, 0.15 and 0.064, respectively. ϕ_u^T was obtained from the theory outlined in §2 of the
289 main text. S_a and V_p are the surface area and the volume of an individual JW3434-MTc cell as
290 computed from the equivalent cell radius *a* obtained from AFM (Section A in ESI). $\rho_S^{V_i} = 12$ mM
291 corresponds to the total concentration of intracellular thiol groups supported by MBP-MT and by the
292 other cytosolic proteins (see ESI text for details). Uncertainties pertaining to the analysis of depletion
293 kinetics (●) correspond to the range of $\bar{K}^*$ values for which the reconstruction of the experimental
294 data are acceptable given the experimental error bars indicated in Figure 1B of the main text. At low
295 $(\phi_u^T S_a / V_p) / \rho_S^{V_i}$ (or high φ), only lower limits of $\bar{K}^*$ are defined for the reason given in the text.
296 Error bars from AGNES measurements (●) correspond to analytical measurement uncertainties.

297

298 **Section G: Construction of a master curve from Cd(II) depletion kinetic data collected**

299 **for JW3434 cells (Figure 1A).**

For bacterial cells deprived of intracellular MTc (*i.e.* $\lambda \ll 1$ and $\bar{K}^* \ll 1$) and in line with applicability of the equilibrium relationship $c_{\mathrm{M}}^{\mathrm{a}}(t) = \beta_a c_{\mathrm{M}}^*(t)$ at any time t (*i.e.* $Bn^{-1} \ll 1$), $c_{\mathrm{M}}^*(t)$ verifies the transcendental equation[9,15]

$$F\left(c_{\mathrm{M}}^*(t), c_{\mathrm{M}}^*\left(0^+\right)\right) = t \tag{S1}$$

, where the function F in the above limits may be written by eqn (S2) obtained after some straightforward arrangements of eqn (2) given in ref[9]

$$F\left(c_{\mathrm{M}}^*(t), c_{\mathrm{M}}^*\left(0^+\right)\right) = \left\{\frac{\varphi^*}{\varphi}\left(1+\frac{c_+}{K_{\mathrm{M}}}\right)\left(1+\frac{c_-}{K_{\mathrm{M}}}\right)\left(\frac{c_+ - c_-}{K_{\mathrm{M}}}\right)\right\}^{-1} \ln\left\{\frac{\left[\dfrac{\beta_a c_{\mathrm{M}}^*(t) - c_-}{\beta_a c_{\mathrm{M}}^*\left(0^+\right) - c_-}\right]^{p_-(1+\bar{c}_+)}}{\left[\dfrac{\beta_a c_{\mathrm{M}}^*(t) - c_+}{\beta_a c_{\mathrm{M}}^*\left(0^+\right) - c_+}\right]^{p_+(1+\bar{c}_-)}}\right\} \tag{S2}$$

, where c_+ (mol m^{-3}) is obtained from eqn (7) taken in the limit $\bar{K}^* \ll 1$. c_- (mol m^{-3}) and $p_\pm$ (s) are defined by $c_- = (x_0 - 2)K_{\mathrm{M}} - c_+$ and $p_\pm = \dfrac{\varphi^*}{k_{\mathrm{e}}\varphi}\left(1+\dfrac{c_\pm}{K_{\mathrm{M}}}\right)^2$. The latter expressions are derived from those given by Duval et *al.*[15] after realizing that the characteristic timescales τ_{L} and τ_{E} therein defined for the M membrane transfer and M transfer from bulk solution to intracellular compartment, respectively, satisfy -under equilibrium condition- the equality $\tau_{\mathrm{E}} = \tau_{\mathrm{L}}$ with $\tau_{\mathrm{L}} = \varphi^* / (k_{\mathrm{e}}\varphi)$ or equivalently $\tau_{\mathrm{L}} = -\tau_{\mathrm{o}} / x_{\mathrm{o}}$,[9] where τ_{o} is defined in[15] for the practical case where there is no intracellular metal species at $t = 0$.

Equation S1 predicts a linear dependence of $F\left(c_{\mathrm{M}}^*(t), c_{\mathrm{M}}^*\left(0^+\right)\right)$ on time t with unit slope, recalling that the equilibrium condition $c_{\mathrm{M}}^*(t) = c_{\mathrm{M}}^{\mathrm{a}}(t)$ applies for JW3434 strain ($Bn^{-1} \ll 1$) with $\beta_a = 1$ (see details in main text and in Section B of ESI). To verify the validity of eqn (S1) (and therewith the consistent data modeling displayed in **Figure 1A**), values of $c_{\mathrm{M}}^*(t)$

and $c_M^*(0^+)$ measured under the φ conditions specified in **Figure 1A** were injected into the expression of F (eqn (S2)) with the relevant values of K_M, k_e and φ^* listed in **Table 1**. Within experimental error, the results provided in **Figure S5** very well agree with theoretical prediction and they highlight that all data in Figure 1A can be projected onto a single master curve whose expression is provided by eqns (S1) and (S2).

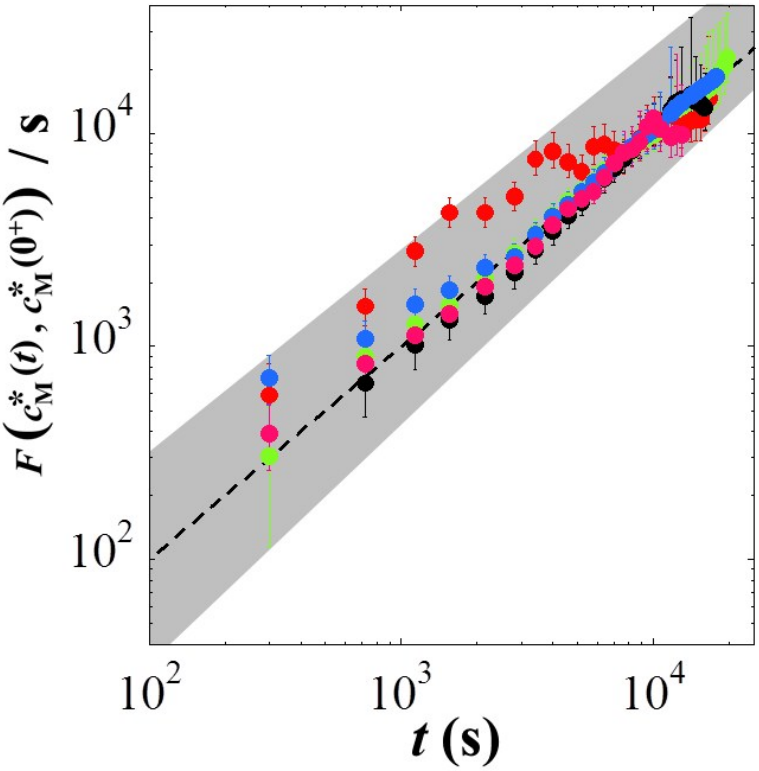

Figure S5. Master curve constructed from the Cd(II) bulk depletion kinetic data provided for JW3434 cells in Figure 1A of the main text (one color corresponds to one given φ condition). See ESI text for details. Error bars pertain to uncertainties on cell volume fractions (estimated at $\pm$ 5%). Data in red dots correspond to the lowest cell volume fraction adopted in Figure 1A ($\varphi = 1.21 \times 10^{-4}$) and they are thus more scattered due to the weaker depletion of Cd(II) concentration in bulk solution. The shaded area brackets all experimental data (including measurement uncertainties).

REFERENCES

1 E. Dague, J.F.L. Duval, F. Jorand, F. Thomas, F. and F. Gaboriaud, *Biophys. J.,* 2006, **90**, 2612–2621.

2 J. F. L. Duval and F. Gaboriaud, *Curr. Opin. Colloid Interface Sci.,* 2010, **15**, 184–195.

3 J. F. L. Duval and H. Ohshima, *Langmuir* , 2006, **22**, 3533–3546.

4 H. Ohshima, *Adv. Colloid Interface Sci.* 1995, ***62***, 189–235.

5 S.C. Monterroso, H.M. Carapuça, J.E. Simão and A.C. Duarte, *Anal. Chim. Acta,* 2004, **503**, 203–212.

6 R.F. Domingos, C. Huidobro, E. Companys, J. Galceran, J. Puy and Pinheiro, *J. Electroanal. Chem.* 2008, **617,** 141–148.

7 C. Parat, L. Authier, D. Aguilar, E. Companys, J. Puy, J. Galceran, J. and M Potin-Gautier, *Analyst,* 2011, **136**, 4337–4343.

8 H.P. Van Leeuwen and R.M. Town, *Environ. Sci. Technol.,* 2003, **37**, 3945–3952.

9 E. Rotureau, P. Billard and J.F.L. Duval, *Environ. Sci. Technol.,* 2015, **49**, 990–998.

10 R. Hajdu, J.P. Pinheiro, J. Galceran and V.I. Slaveykova, *Environ. Sci. Technol.,* 2010, **44**, 4597–4602.

11 M.M. Bradford, *Anal. Biochem.,* 1976, **72**, 248–254.

12 S.P. Lavoie, D.T. Mapolelo, D. M. Cowart, B.J. Polacco, M.K. Johnson, R.A. Scott, S.M. Miller and A.O. Summers, *J. Biol. Inorg. Chem.,* 2015, **20**, 1239–1251.

13 H. Lodish, A. Berk, P.Matsudaira , C.A. Kaiser, M. Krieger, M.P. Scott, L. Zipursky and J. Darnell. In *Molecular Cell Biology*, W.H. Freeman and co, New-York,5th edition, 2003, chapt.7, 245-300

14 J.F.L. Duval, R.M. Présent, E. Rotureau, *Phys. Chem. Chem. Phys.,* 2016, **18**, 30415–30435.

15 J.F.L. Duval, E. Rotureau, *Phys. Chem. Chem. Phys.,* 2014, **16**, 7401–7416.